Tsunami scenario triggered by the activity of the Mentawai Fault Zone offshore western Sumatra Island

Haekal A. Haridhi[1,2,3,*], *Ichsan* Setiawan[2,3], *Chitra* Octavina[2,3], *Saiful* Mahdi[2,3], *Cut Putrie* Balqies[2,3]

[1]Tsunami and Disaster Mitigation Research Center (TDMRC), Universitas Syiah Kuala, Banda Aceh 23111, Indonesia
[2]Research Center for Marine Sciences and Fisheries, Universitas Syiah Kuala, Banda Aceh 23111, Indonesia
[3]Department of Marine Sciences, Faculty of Marine and Fisheries, Universitas Syiah Kuala, Banda Aceh 23111, Indonesia

Abstract. Subduction zones worldwide pose tsunami risks, mainly linked to megathrust activity near subduction trenches. However, tsunamis can originate from various sources, including marine volcanic eruptions, submarine landslides, and strike-slip earthquakes. In the Sumatra subduction zone, a seismic gap in the Mentawai region heightens the tsunami risk. This region's tectonics are complex due to the oblique subduction of the India-Australia oceanic plate beneath the Eurasian continental plate, leading to the sliver faults system of Mentawai Fault Zone (MFZ) and Sumatra Fault Zone (SFZ). The SFZ on Sumatra Island has limited tsunami potential, except at its northern and southern offshore extensions. In contrast, the MFZ, situated in the marine Northern Bengkulu basin, holds a higher tsunami-generation potential. This study aims to assess the MFZ activity in generating tsunamis, estimate the maximum wave height, and analyze propagation, and arrival times at several crucial sites in Western Sumatra Province. We utilized the COMCOT tsunami model to simulate scenarios with two fault mechanisms, i.e., strike-slip and back thrust, and two magnitudes (Mw 7.6, and 8.2). The results indicate that the most hazardous tsunami, generated by a strike-slip fault with Mw 8.2, produces a 2-meter tsunami on the east coast of Siberut Island and the west coast of Padang City, West Sumatra. The scenarios reveal that Mentawai Island's eastern part lacks evacuation time, with an almost instantaneous tsunami arrival. In contrast, western Sumatra, including Pariaman and Padang City, has 13 to 20 minutes for evacuation planning. Thus, disaster risk reduction strategies in these locations should consider these findings.

1 Introduction

The Sumatra Island is renowned as one of the world's most seismically active regions [1]. The historical record attests to a plethora of seismic events and tsunami occurrences resulting from the intricate interplay of convergent plate boundaries within the Sumatra subduction zone [2–4]. This subduction zone is where the Indo-Australian oceanic plate subduct beneath the Eurasian plate [1].

Present-day seismotectonics in Sumatra are primarily governed by three major fault systems: the Sumatra subduction zone (comprising thrust and splay faults), the Sumatra Fault Zone (SFZ) (exhibiting strike-slip right lateral movement), and the Mentawai Fault Zone (MFZ) (also characterized by strike-slip right lateral motion) [1,5,6].

Along the Sumatra subduction zone, a seismic gap has been identified [7,8], a region with a lower occurrence of earthquake activities, situated in the Mentawai region, known as the Mentawai seismic gap. Recent studies on this seismic gap have indicated the potential for an earthquake of a magnitude similar to that of the Indian Ocean Tsunami (IOT) mega earthquake and tsunami [9].

The historical record indicates that two tsunamis occurred, one in 1797 with a magnitude (Mw) ranging between 8.7 – 8.9, and another in 1833 with a magnitude Mw 8.9 – 9.1. These events generated tsunamis exceeding 6 meters height in the coastal regions of West Sumatra and Bengkulu region [10].

Thus, based on the historical tsunami record in the Mentawai region and the presence of the Mentawai gap, it is important to mitigate the tsunami hazard in this region. While important studies have been conducted regarding the tsunami hazard in this area, they have primarily focused on modelling using the major thrust and splay fault system within the subduction zone as the tsunami generator [11]. However, the potential of the marine MFZ to generate tsunamis remains less studied. Therefore, this study aims to assess the MFZ activity in generating tsunami, evaluate the maximum tsunami height, and analyse propagation and arrival times at several crucial sites in Western Sumatra Province.

Recent studies on the movement of the MFZ have not reached a conclusive understanding. There are two models related to the MFZ activities: one involves strike-slip with right lateral movement [1,6], and the other involves back thrust [12]. To emphasize the significance of tsunami hazard mitigation, this study considers these two mechanisms as potential tsunami generators along the MFZ. Recent seismic activity records between 2000 – 2023 from the USGS catalog (https://earthquake.usgs.gov/earthquakes/) indicate a

* Corresponding author: haekal.azief.haridhi@usk.ac.id

total of 203 earthquake events with magnitude ranging between 5 to 7.9 occurred in this region.

To model the tsunami in this study, we utilize the Cornell Multi-grid Tsunami Model (COMCOT) [13]. The COMCOT model has been widely employed for modeling and validating tsunamis worldwide [14–21].

2 Tectonic setting of Sumatra

The Sumatra subduction zone arises from the convergence of large tectonic plates (see Fig. 1.1a). The Australian plate descends obliquely beneath the Eurasian plate, with convergence rates varying from 50 to 70 mm/yr along the trench, spanning from north to south [1]. This convergence finds expression in the dip-slip action of the subduction interface, recognized as the megathrust, and the lateral right-shift motion on Sumatra Island, manifest as the Sumatra Fault Zone (SFZ) [5,22,23]. In the oceanic plate, reactivated Fracture Zones (FZ) displaying lateral left-shift movement influence seismic activity distribution within the subduction zone [24,25].

Of notable significance is the hazardous and tsunami-prone stretch within the Sumatra accretionary prism. Here, a cluster of trench-aligned thrust and splay faults has been identified as the origin of tsunamis [24–26]. Furthermore, an unreleased seismic tension, demarcated by the term "GAP" in Fig. 1a, characterizes the Mentawai section of the megathrust.

Prominently demarcating Sumatra Island (see Fig. 1a) is the SFZ, spanning about 1,900 km from the Sunda Strait to Banda Aceh. The fault line of the SFZ associates with a sequence of valleys along the mountain range [5]. Notably, the SFZ's continuity fluctuates between the south and north; it is fragmented into distinct segments. This segmentation of the SFZ also influences the partitioning of earthquakes and serves as a rupture barrier, limiting the potential magnitude of seismic events [27].

The presence of these two significant sliver plate faults, characterized by right-lateral movement, serves to compensate for the oblique subduction [6]. Notably, unlike the SFZ, which is situated on land, the MFZ is situated entirely beneath the sea. It's worth mentioning that [12] proposed an alternative interpretation, suggesting a back thrust mechanism for the MFZ.

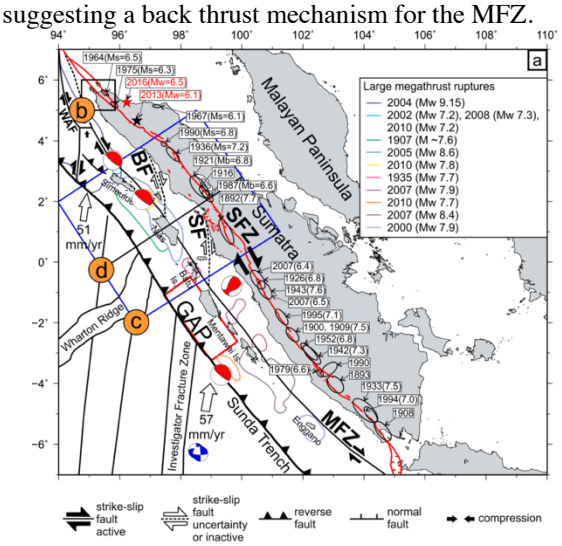

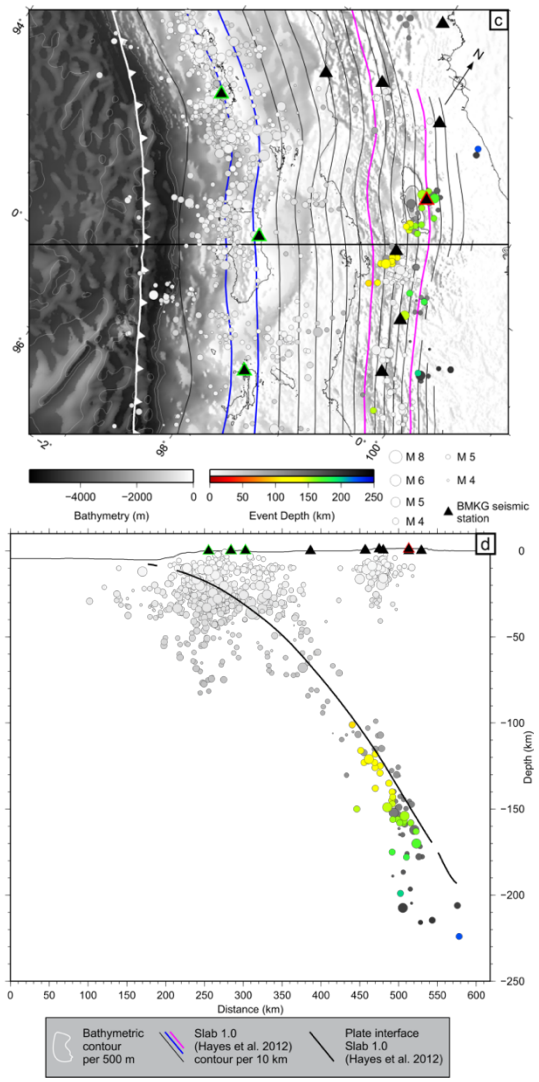

Fig. 1. The seismotectonic background along the Sumatra subduction zone is based on seismic data collected from the ISC and refined BMKG catalogs [7], along with focal mechanism data retrieved from the Global CMT catalog (http://www.globalcmt.org/). (a) Sumatra's tectonic setting, as interpreted by [6], is depicted. The areas prone to large megathrust ruptures are identified in the text [28]. The solid red line represents the SFZ, with historical earthquake locations and approximate rupture areas identified by [5]. Red focal mechanisms denote significant earthquake sequences at the Sumatra subduction zone post the 2004 Indian Ocean Tsunami (IOT), while blue focal mechanisms indicate activity along the oceanic Fracture Zone (FZ). The Mentawai gap is marked with the text "GAP" and a red square box to indicate its location. Labels “c” correspond to the enlarged map (c), and label “d” represents the cross-section shown in (d). (c) The grayscale representation shows seismic activity in the central portion of Sumatra from 1993 to 2011. Another color scale represents intermediate earthquakes covering the period between 2013 and 2018. (d) A cross-section plot of the central portion of the Sumatra subduction zone is displayed. Topographic highs are depicted by thin solid black lines. The plot includes information about fault mechanisms, earthquake sizes, seismic stations, topography, and subducting slab contours [29].

3 Data and Method

3.1 Numerical simulation

A tsunami wave propagation model was created by simulating it using the Cornel Multi-grid Coupled Tsunami (COMCOT) model, developed by [13]. This model has been successfully used in various tsunami scenarios, including the IOT case [15] and the Tohoku Earthquake and Tsunami. The COMCOT model can simulate grids of different sizes using a nested grid method. It employs a leap-frog finite difference scheme and utilizes two modes of the Boussinesq-Shallow Water Equation (SWE): a linear SWE and a nonlinear SWE [13,30].

As tsunami waves travel from offshore to near-shore areas, the influence of nonlinear effects becomes significantly more pronounced. However, applying a nonlinear SWE for the entire simulation domain is inefficient and time-consuming. The advantage of COMCOT is its capability to selectively apply different types of equations in different parts of the simulated area, allowing for a more efficient and effective simulation [16].

In simulating the tsunami in this study, the detail information on the nested grid used in this study is presented in Table 1 and its geographical distribution is illustrated in Fig. 2.

Table 1. The Layer properties applied for COMCOT in this study.

Layer	Coordinate Position in °		Grid Properties		SWE Type
	Lon	Lat	Size (minute)	Number	
1	93.03	-5.16	1	540	Linear
	101.96	3.86		546	
2	96.16	-4.13	0.5	636	Linear
	101.43	1.88		726	
3	97.01	-3.64	0.25	984	Linear
	101.09	0.99		1116	
4	97.40	-3.39	0.125	1622	Linear
	100.77	0.27		1766	
5	98.50	-1.89	0.06	1920	Non-linear
	100.49	-0.50		1344	

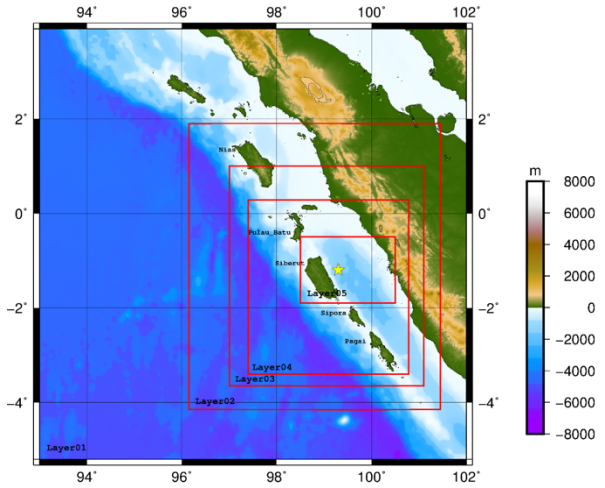

Fig. 2. The spatial distribution of each layer used in the COMCOT model.

3.2 Simulation scenario

In this research, we created and simulated 4 scenarios using two different earthquake fault mechanisms: strike-slip and back thrust. We collected magnitude data from the National Earthquake Study Center (Pusgen) and the United States Geological Survey (the USGS). The important information related to the scenarios is represented in Table 2.

Table 2. Tsunami scenarios.

Scenario	Fault Mechanism	Earthquake Magnitude (Mw)
1	Back thrust	7.6
2	Strike-slip	7.6
3	Back thrust	8.2
4	Strike-slip	8.2

4 Result and Discussion

4.1 Result

4.1.1 Initial condition

a. Scenario 1

In scenario 1, the results indicate that the fault rupture extends from the northern part of Siberut Island to the southern part of Siberut Island. The initial wave conditions for tsunami scenario 1 are displayed in Fig. 3.

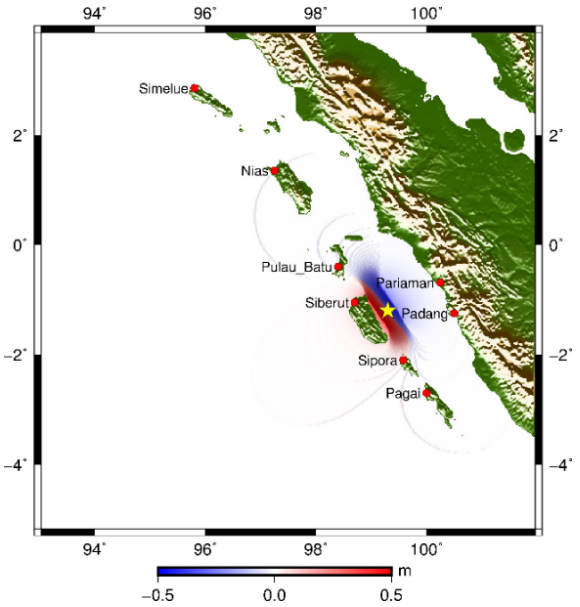

Fig. 3 Initial condition of tsunami wave at layer 1.

b. Scenario 2

In scenario 2, the results show a longer fault rupture compared to scenario 1. The initial wave conditions for tsunami scenario 2 are displayed in Fig. 4.

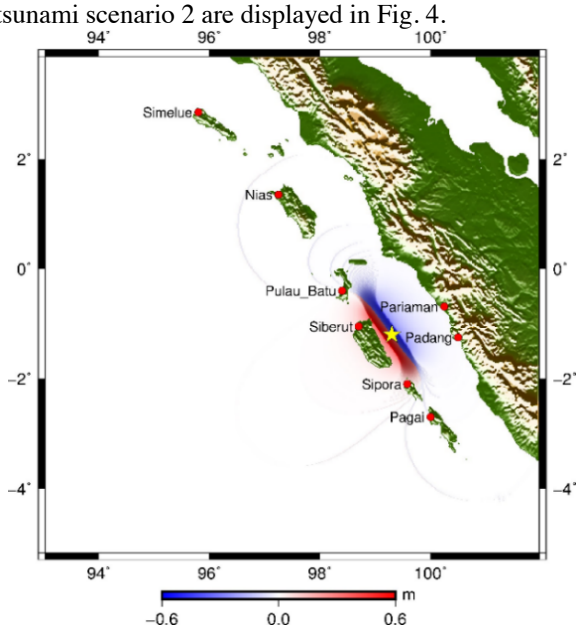

Fig. 4. Same as Fig. 3, but for scenario 2.

c. Scenario 3

The initial wave conditions for tsunami scenario 3 indicate that the earthquake fault rupture extends as far as Batu Islands and Sipora Island. The simulation results are displayed in Fig. 5.

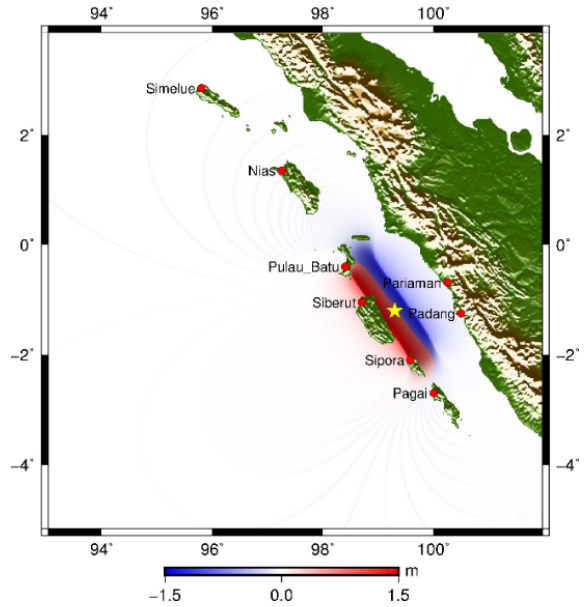

Fig. 5. Same as Fig. 3, but for scenario 3.

d. Scenario 4

The initial wave conditions for tsunami scenario 4 depict a broader fault rupture compared to scenario 3. In scenario 4, the earthquake rupture extends beyond Batu Islands, reaching the northern part of Pagai Island. The simulation results for the initial wave conditions of scenario 6 can be seen in Fig. 6.

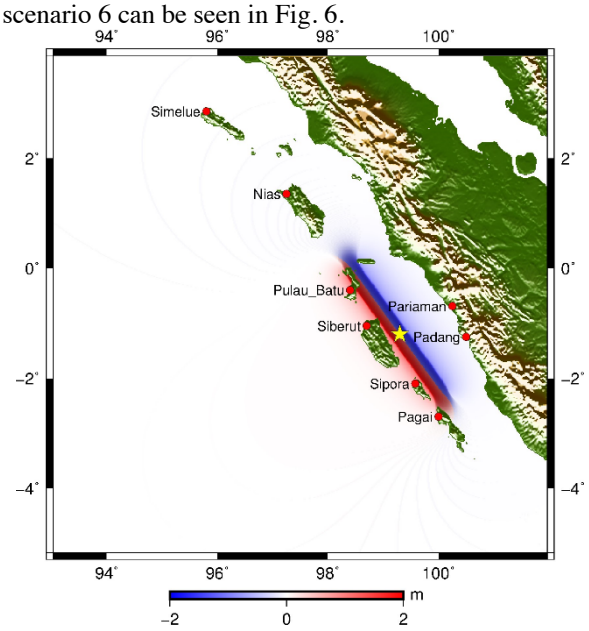

Fig. 6. Same as Fig. 3, but for scenario 4.

4.1.2 Propagation of tsunami wave

a. Scenario 1

The tsunami wave simulation for scenario 1 resulted in a wave height of approximately 0.5 meters. The simulation results for the propagation of the tsunami wave in scenario 1 can be observed in Fig. 7.

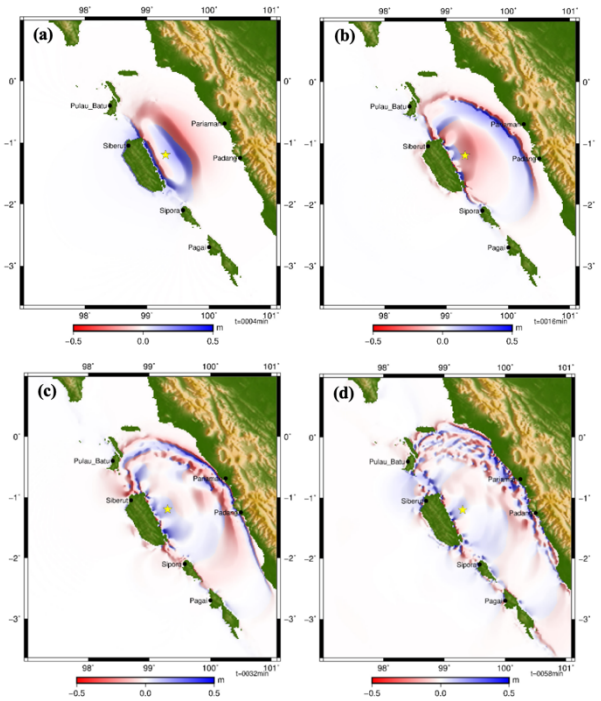

Fig. 7. Snapshot of tsunami wave propagation in scenario 1. (a) 4 minutes, (b) 20 minutes, (c) 34 minutes, and (d) 58 minutes.

b. Scenario 2

The tsunami wave simulation for scenario 2 resulted in a wave height of approximately 0.6 meters. The simulation results for scenario 2 can be observed in Fig. 8.

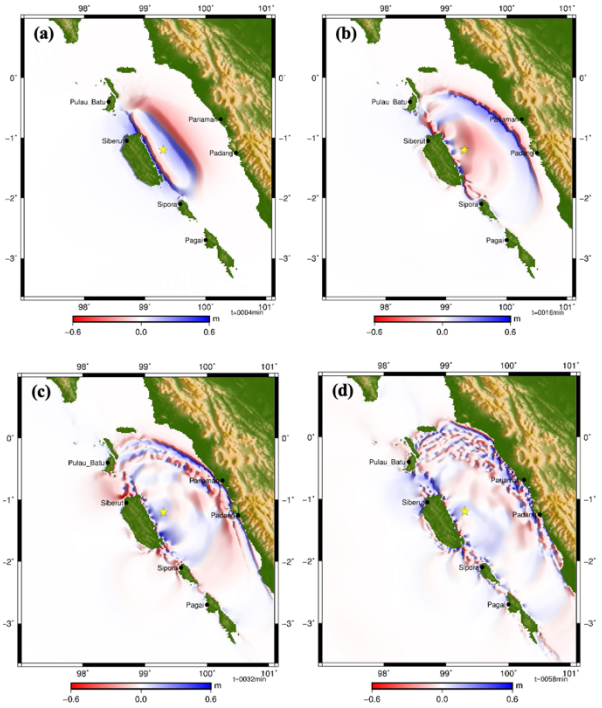

Fig. 8. Same as Fig. 7 but for scenario 2.

c. Scenario 3

The tsunami wave simulation for scenario 3 resulted in a wave height of approximately 1.5 meters. The simulation results for the propagation of the tsunami wave in scenario 5 can be observed in Fig. 9.

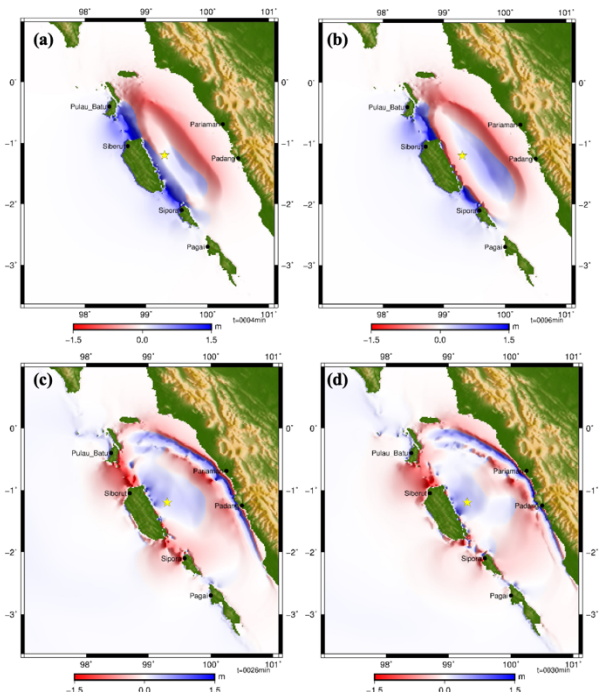

Fig. 9. Same as Fig. 7 but for scenario 3.

d. Scenario 4

The tsunami wave simulation for scenario 4 resulted in a wave height of approximately 2 meters. The simulation results for the propagation of the tsunami wave in scenario 4 can be observed in Fig. 10.

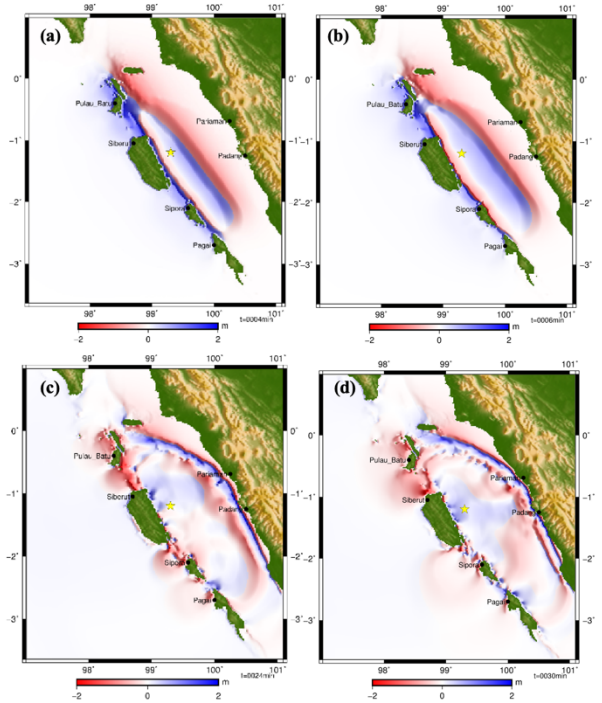

Fig. 10. Same as Fig. 7 but for scenario 4.

4.1.3 Tsunami wave height and arrival time

a. Scenarios 1 and 2

The tsunami wave heights in scenarios 1 and 2 had an impact on the coast of West Sumatra and Siberut. However, the tsunami waves were not very significant because the maximum wave height generated by both scenarios was approximately 0.5 – 0.6 meters. The wave

height results for scenarios 1 and 2 can be seen in Fig. 11.

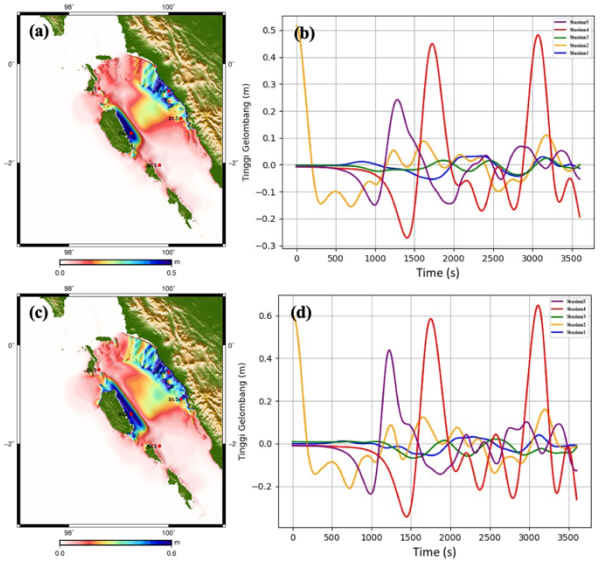

Fig. 11. Wave heights for scenarios 1 and 2 are depicted as follows: (a) shows the wave height for scenario 1, (b) displays a time series graph for scenario 1, (c) illustrates the wave height for scenario 2, and (d) presents a time series graph for scenario 2.

b. Scenarios 3 and 4

In scenario 3, the tsunami wave had an impact on the western coast of West Sumatra, as well as on Siberut Island, Sipora Island, and Batu Island, reaching a maximum wave height of around 1.50 meters. In scenario 4, the tsunami wave affected the western coast of West Sumatra and nearly the entire Mentawai Islands, resulting in a maximum wave height of approximately 2 meters. The difference in maximum wave height between scenarios 3 and 4 was approximately 0.50 meters. You can view the simulation results for the wave heights in scenarios 3 and 4 in Fig. 12.

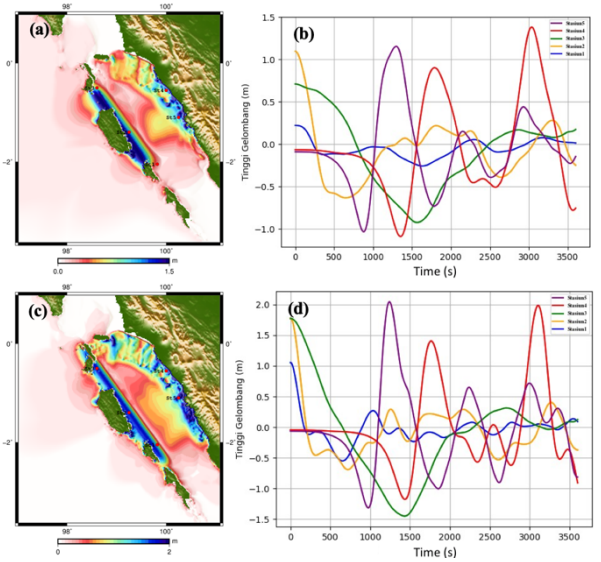

Fig. 12. Same as Fig. 11 but for scenario 3 and 4.

4.2 Discussion

Based on the tsunami wave impacts on the coastal areas of West Sumatra and its vicinity originating from back thrust mechanisms with Mw 7.6, and 8.2, varying wave heights were generated, resulting in different outcomes [11,31]. The region's most vulnerable to tsunami wave impacts are Siberut Island, Batu Islands, Pariaman, and Padang. This susceptibility arises due to the proximity of these areas to the seismic source, causing earlier wave arrival compared to more distant stations [15].

In contrast, the tsunami wave impacts on the coastal areas of West Sumatra and its vicinity from strike-slip mechanisms with Mw 7.6 and 8.2 produced higher tsunami waves than back thrust mechanisms. Despite using the same magnitudes, the resulting fault areas differ. Stations (St) 2, St 4, and St 5 are the most severely affected areas by tsunami waves. As tsunami waves approach land, their height increases. The nearshore tsunami height experiences amplification due to water mass accumulation caused by reduced propagation opportunity, resulting in significantly higher tsunami wave heights upon reaching the coastal areas compared to the wave heights at the earthquake epicenter [15,19].

Tsunami wave modeling in the West Sumatra region (Painan) has also been simulated by [11], where tsunami waves originating from the MFZ directly impact the areas of West Sumatra, Mentawai, and surrounding regions. In contrast to the Haiti case modeled by [32], tsunami waves propagating southwest of Mentawai hinder the tsunami wave propagation towards West Sumatra. This is due to the Mentawai Islands acting as a barrier during a tsunami event, preventing its impact on West Sumatra.

From the findings of this research, recommendations include the necessity of implementing mitigation measures, both non-structural and structural. These measures could involve constructing evacuation buildings in tsunami-prone nearshore areas and strengthening coastal infrastructure to reduce inundation. The data from this study is expected to serve as a foundation and information source for enhancing the awareness of coastal communities regarding the potential occurrence of tsunamis at any time, thereby minimizing the impact and facilitating self-rescue measures.

5 Conclusion

Based on the results of this research, the following conclusions can be drawn:

a. The simulation results from the two fault mechanisms in the MFZ region show varying tsunami wave outcomes.
b. The maximum tsunami heights along the coast of West Sumatra and its vicinity in scenarios 1 and 2 resulted in wave heights of approximately 0.5-0.6 meters, scenario 3 produced wave heights of about 0.50 meters, scenario 4 yielded wave heights of around 0.60 meters, scenario 5 generated wave heights of approximately 1.50 meters, and scenario 6 resulted in wave heights of around 2 meters.
c. The areas estimated to be most severely impacted by tsunami waves are Siberut Island and the west coast of West Sumatra.

These findings provide valuable insights into the potential variations in tsunami wave heights and their impacts on specific coastal regions, thereby contributing to enhanced preparedness and mitigation efforts in tsunami-prone areas.

Acknowledgements: We would like to express our sincere gratitude to Prof. Syamsidik at TDMRC USK and Dr. T. Rasyif at Bakrie University for their invaluable support and guidance in implementing the COMCOT tsunami model. Our heartfelt thanks go to Mr. Ibrahim, Ms. Tursina, and Ms. Nurfadillah for their generous assistance during the Training Tsunami Model using COMCOT, a collaborative initiative between TDMRC and the Research Center for Marine Sciences and Fisheries at Universitas Syiah Kuala. This research received funding from the Ministry of Education, Culture, Sciences, and Technology of the Republic of Indonesia, specifically through the Institute of Research and Community Service (LPPM) at Universitas Syiah Kuala, as part of the Research Center for Marine Sciences and Fisheries' involvement in the Penugasan Penelitian Pusat Riset Katagori B scheme. We also utilized the Generic Mapping Tools software package for creating map figures [33].

References

1. A. J. Barber and J. S. Milsom, *(Eds) Sumatra: Geology, Resources and Tectonic Evolution* (Geological Society of London, Oxford, 2005)
2. K. R. Newcomb and W. R. McCann, J. Geophys. Res. **92**, 421 (1987)
3. A. J. Meltzner, K. Sieh, M. Abrams, D. C. Agnew, K. W. Hudnut, J. P. Avouac, and D. H. Natawidjaja, J. Geophys. Res. **111**, B02407 (2006)
4. K. Sieh, D. H. Natawidjaja, A. J. Meltzner, C.-C. Shen, H. Cheng, K.-S. Li, B. W. Suwargadi, J. Galetzka, B. Philibosian, and R. L. Edwards, Science (80-.). **322**, 1674 (2008)
5. K. Sieh and D. Natawidjaja, J. Geophys. Res. **105**, 28295 (2000)
6. K. Berglar, C. Gaedicke, S. Ladage, and H. Thöle, Tectonophysics **710–711**, 225 (2017)
7. H. A. Haridhi, B.-S. Huang, K.-L. Wen, D. Denzema, R. A. Prasetyo, and C.-S. Lee, Terr. Atmos. Ocean. Sci. **29**, 635 (2018)
8. M. Chlieh, J. P. Avouac, K. Sieh, D. H. Natawidjaja, and J. Galetzka, J. Geophys. Res. **113**, B05305 (2008)
9. T. Lay, Earth Planet. Sci. Lett. **409**, 133 (2015)
10. D. H. Natawidjaja, K. Sieh, M. Chlieh, J. Galetzka, B. W. Suwargadi, H. Cheng, R. L. Edwards, J. Avouac, and S. N. Ward, J. Geophys. Res. **111**, B06403 (2006)
11. L. Li, Z. Huang, Q. Qiu, D. H. Natawidjaja, and K. Sieh, Earth, Planets Sp. **64**, 799 (2012)
12. S. C. Singh, N. D. Hananto, A. P. S. Chauhan, H. Permana, M. Denolle, A. Hendriyana, and D. Natawidjaja, Geophys. J. Int. **180**, 703 (2010)
13. P. L.-F. Liu, Y.-S. Cho, M. J. Briggs, U. Kanoglu, and C. E. Synolakis, J. Fluid Mech. **302**, 259 (1995)
14. T. Wu, P. Chen, W. Tsai, and G. Chen, Terr. Atmos. Ocean. Sci. **19**, 705 (2008)
15. T. M. Rasyif, S. Syamsidik, M. Al'ala, and M. Fahmi, J. Coast. Conserv. **20**, 489 (2016)
16. Syamsidik, T. M. Rasyif, and S. Kato, Int. J. Disaster Risk Reduct. **14**, 403 (2015)
17. Syamsidik, M. Al'Ala, H. M. Fritz, M. Fahmi, and T. Hafli Mudi, Nat. Hazards Earth Syst. Sci. **19**, 1265 (2019)
18. Syamsidik, Tursina, A. Meutia, M. Al'ala, M. Fahmi, and E. Meilianda, J. Earthq. Tsunami **11**, 1 (2017)
19. T. M. Rasyif, S. Kato, Syamsidik, and T. Okabe, Geosci. **9**, 1 (2019)
20. L. Li, Q. Qiu, and Z. Huang, Nat. Hazards **64**, 1549 (2012)
21. H. A. Haridhi, B. S. Huang, K. L. Wen, A. Mirza, S. Rizal, S. Purnawan, I. Fajri, F. Klingelhoefer, C. S. Liu, C. S. Lee, C. R. Wilson, T. Wu, I. Setiawan, and V. B. Phung, Nat. Hazards Earth Syst. Sci. **23**, 507 (2023)
22. R. Collings, D. Lange, A. Rietbrock, F. Tilmann, D. Natawidjaja, B. Suwargadi, M. Miller, and J. Saul, J. Geophys. Res. **117**, B01312 (2012)
23. C. Subarya, M. Chlieh, L. Prawirodirdjo, J. Avouac, Y. Bock, K. Sieh, A. J. Meltzner, D. H. Natawidjaja, and R. McCaffrey, Nature **440**, 46 (2006)
24. J. Y. Lin, X. Le Pichon, C. Rangin, J. C. Sibuet, and T. Maury, Geochemistry, Geophys. Geosystems **10**, Q05006 (2009)
25. J. C. Sibuet, C. Rangin, X. Le Pichon, S. Singh, A. Cattaneo, D. Graindorge, F. Klingelhoefer, J.-Y. Lin, J. Malod, T. Maury, J.-L. Schneider, N. Sultan, M. Umber, and H. Yamaguchi, Earth Planet. Sci. Lett. **263**, 88 (2007)
26. T. Lay, C. J. Ammon, H. Kanamori, Y. Yamazaki, K. F. Cheung, and A. R. Hutko, Geophys. Res. Lett. **38**, L06302 (2011)
27. D. Lange, F. Tilmann, T. Henstock, A. Rietbrock, D. Natawidjaja, and H. Kopp, Solid Earth **9**, 1035 (2018)
28. A. J. Meltzner, K. Sieh, H. Chiang, C. Shen, B. W. Suwargadi, D. H. Natawidjaja, B. Philibosian, and R. W. Briggs, J. Geophys. Res. **117**, B04405 (2012)
29. G. P. Hayes, G. L. Moore, D. E. Portner, M. Hearne, H. Flamme, M. Furtney, and G. M. Smoczyk, Science (80-.). **362**, 58 (2018)
30. X. Wang, Https://Pdfs.Semanticscholar.Org/401d/E93588d6c28d0c3984044ad1f95b75dadab0.Pdf (2009)
31. Syamsidik and D. C. Istiyanto, J. Earthq. Tsunami **7**, (2013)
32. A. Poupardin, E. Calais, P. Heinrich, M. Rodriguez, S. Leroy, H. Aochi, and R. Douilly, Nat. Hazards Earth Syst. Sci. **20**, 2055 (2020)
33. P. Wessel and W. H. F. Smith, Eos, Trans. Am. Geophys. Union **79**, 579 (1998)